IEEE Access
Multidisciplinary | Rapid Review | Open Access Journal

Received 14 April 2023, accepted 27 April 2023, date of publication 1 May 2023, date of current version 10 May 2023.

*Digital Object Identifier 10.1109/ACCESS.2023.3272112*

RESEARCH ARTICLE

# Impact of Secondary Control Design on the Microgrid Domain of Stability Considering Reactive Power Sharing

**AHMED LASHEEN[1], HATEM F. SINDI[2], (Senior Member, IEEE), MAJID NOUR[3], MOSTAFA F. SHAABAN[4], (Senior Member, IEEE), AHMED OSMAN[4], (Senior Member, IEEE), AND HATEM H. ZEINELDIN[1], (Senior Member, IEEE)**

[1]Department of Electrical Power Engineering, Faculty of Engineering, Cairo University, Cairo 12613, Egypt
[2]Department of Electrical and Computer Engineering, King Abdulaziz University, Jeddah 21589, Saudi Arabia
[3]Department of Biomedical Engineering, King Abdulaziz University, Jeddah 21589, Saudi Arabia
[4]Department of Electrical Engineering, American University of Sharjah, Sharjah, United Arab Emirates

Corresponding author: Ahmed Lasheen (ahmed_lasheen59@cu.edu.eg)

This work was supported by the Deputyship for Research and Innovation, Ministry of Education in Saudi Arabia through the Project 1290.

**ABSTRACT** The basic objective of microgrid primary control is to preserve microgrid stability. On the other hand, microgrid secondary control has been proposed for ensuring reactive power-sharing and restoring the frequency and voltages of the microgrid. Therefore, this paper presents a complete model for evaluating the combined impact of primary and secondary control actions on microgrid domain of stability since the impact of the secondary control design on the domain of stability of the microgrid has not been addressed. Further, the developed model is used to assess the impact of reactive power-sharing, secondary controller design parameters, and communication delay on the domain of stability of the microgrid. The domain of stability is a supportive tool for determining the stable operating range for different microgrid droops. Simulation results have been obtained to validate the developed model and the domain of stability analysis. These results demonstrated that secondary control actions have a significant influence on the domain of stability of the microgrid, and thus it is important to consider the secondary control design in the determination of the microgrid's stable range. Moreover, it has been demonstrated that primary control gains can be severely constrained by reactive power sharing gains.

**INDEX TERMS** Secondary voltage control, frequency control, secondary control, small signal analysis.

## NOMENCLATURE

| | |
|---|---|
| DG | Distributed generator. |
| SSM | Small signal model. |
| RPS | Reactive power sharing. |
| DOS | Domain of stability. |
| IBDG | Inverter-based distributed generator. |
| LHS | Left hand side. |
| PD | Proportional-derivative controller. |
| PI | Proportional-integral controller. |
| $m_P$ | Active droop gain. |
| $n_q$ | Reactive droop gain. |
| $k_d$ | Reactive derivative gain. |
| $\omega$ | Microgrid frequency. |
| $\omega_n$ | No load frequency. |
| $V_n$ | No load voltage. |
| $\Delta\omega_{ns}$ | Secondary frequency control action. |
| $\Delta V_{ns}$ | Secondary voltage control action. |
| $\tau$ | Communication delay. |
| $k_{ws}$ | Secondary frequency gain. |
| $k_{vs}$ | Secondary voltage gain. |
| $k_{qs}$ | Reactive power sharing gain. |
| P | Active power. |
| Q | Reactive power. |

The associate editor coordinating the review of this manuscript and approving it for publication was Nagesh Prabhu.

## I. INTRODUCTION

Renewable energy sources are widely used worldwide to produce electricity due to their economic and environmental

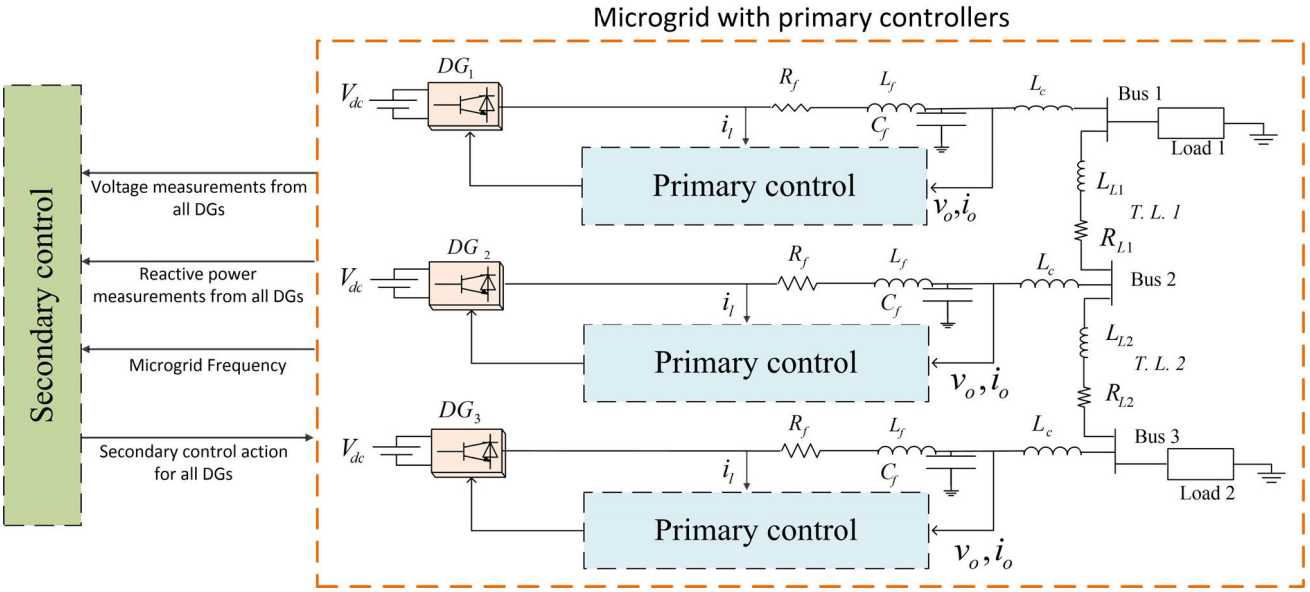


**FIGURE 1.** Schematic diagram of the microgrid model.

advantages [1], [2]. Moreover, the incorporation of distributed generation (DG) has been growing widely in the past few years as they provide several technical and economic benefits for both customers and distribution networks' operators [3]. Microgrids present the building blocks of active distribution networks as per IEEE standard 1547.4. A microgrid can operate in two different forms: autonomously (islanded) and in connection with the grid [4], [5]. In the autonomous mode, the microgrid's main goal is to continuously supply loads while controlling the voltage and the frequency within the microgrid at acceptable levels [6]. The main challenge of the islanded microgrid is to maintain microgrid stability during normal and abnormal conditions. However, in the grid-connected mode, the microgrid absorbs/injects reactive and active power from/into the main grid [1] and [7].

Hierarchical control is made up of three control layers: primary, secondary, and tertiary. The controller in the primary control layer is responsible for improving the transient performance, sharing equal active power across all DGs, and stabilizing the voltage and frequency [1]. Droop controller is the most common approach used in this layer [9], [10]. The controller in the secondary control layer is responsible for removing the offset in the voltage and frequency caused by the primary controller [11], [12]. The controller at the tertiary layer is responsible for managing the flow of power between the main grid and the microgrid [6].

Stability of the microgrid mainly depends on the design of the power controller's droop gain [13], [14]. In [13], it is shown that, through a detailed model, the droop controller of an isolated microgrid is the main controller that determines the dominant pole and thus, it is consequently the main parameter that decides the stability of the microgrid. In the literature, several methods have been proposed that introduce modifications to the structure of the droop controller to enhance the microgrid stability. In [15], a power filter is optimally designed considering the traditional droop controller to improve the microgrid stability. In [16], cascaded lead compensators are proposed for the active droop to enhance the microgrid stability. The microgrid stability enhancements are assessed considering the addition of one, two and three compensators. In [17], decentralized adaptive controller is proposed for the reactive and active droop controllers. The proposed controller improves the transient performance and the microgrid stability significantly. In addition to adaptively varying the droop gains, the method proposed the use of a proportional-derivative (PD) for the droop controller to enhance the transient performance, and the enhancement in stability is assessed through small-signal model (SSM) analysis. All the above methods focus on microgrid primary control for evaluating the microgrid stability.

For the secondary controller, the main target is to regulate the frequency and voltage to their rated values [18], [19], [20]. In [6], the secondary controller decision for voltage and frequency regulation depends on the feedback signals from all DGs. In [18], a cooperative secondary voltage and frequency control strategy are introduced by utilizing an event-triggered approach. This approach depends on the measurement error to produce the control event to maintain the frequency and voltage. In [19], a secondary control structure is introduced for voltage restoration and precise power allocation in islanded microgrids. The proposed secondary controller is designed based on a PI controller to maintain the bus voltages at their rated values. In [20], a nonlinear robust voltage controller is introduced to enhance the bus voltages in the islanded microgrid. Recent work analyzed the influences of

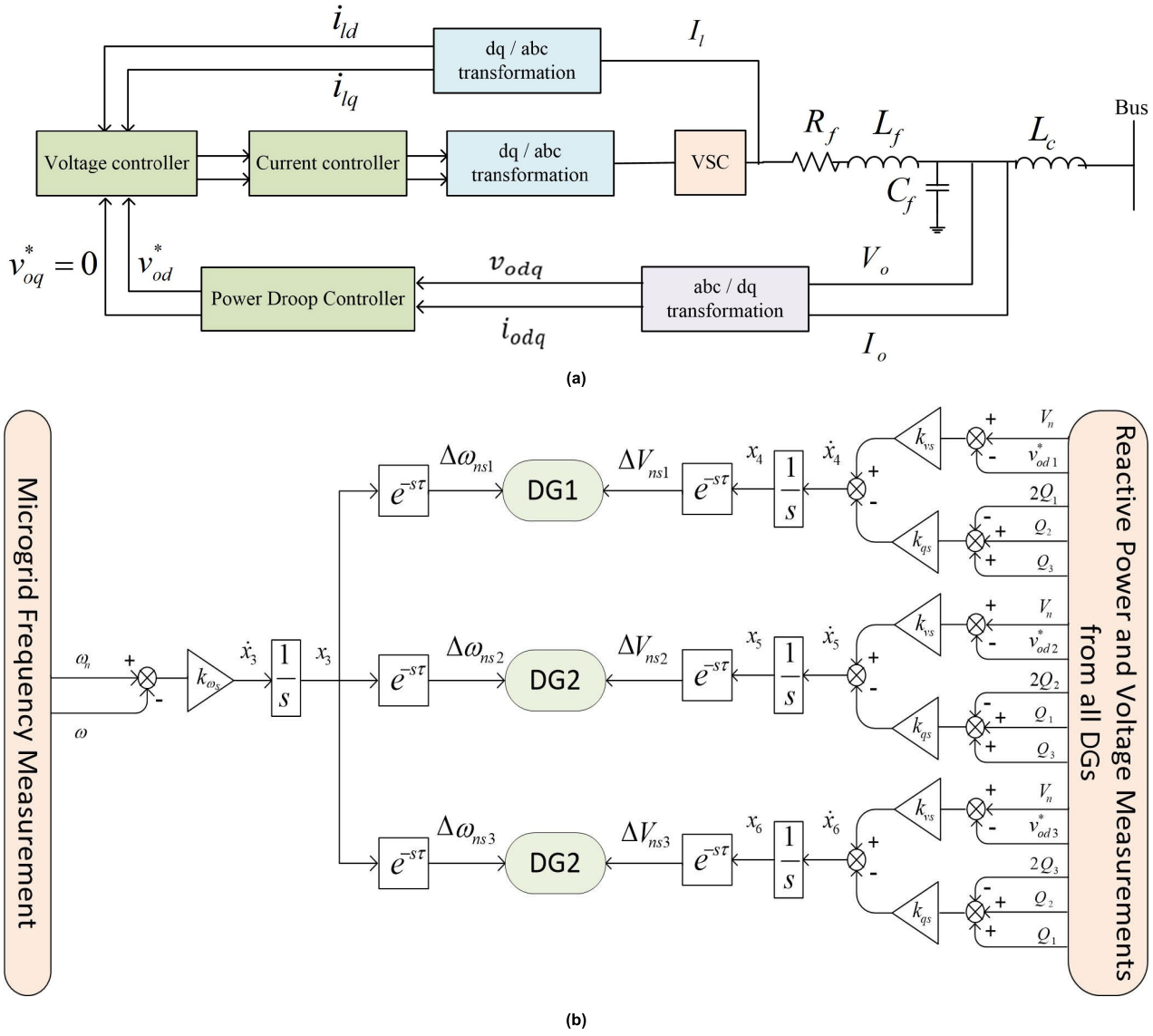


**FIGURE 2.** Detailed structure of the proposed controller (a) primary control structure (b) secondary control structure.

communication delay on the performance of the secondary controller. A relationship between the secondary frequency control parameters and the delay boundaries is obtained [21]. In [22], a tradeoff-based controller for voltage restoration and reactive power sharing (RPS) is discussed, where it has been shown that the higher integral gains would yield fewer delay-dependent stability. In [23], the voltage and power sharing of DGs is improved using a predictive voltage hierarchical controller. In this paper, the primary controller is designed with an inner-loop robust control, ensuring reliable voltage tracking. Further, a predictive controller is developed to provide local and neighbor forecasts.

All the aforementioned methods for assessing the impact of secondary control either: 1) utilize a simplified small-signal stability model to evaluate the influence of secondary control on time-delay while neglecting the impact of the interaction between primary and secondary droop gains, or 2) do not take into account frequency, voltage, and power-sharing as secondary control functions simultaneously in the overall analysis. This paper aims to fill this gap by developing a generalized and detailed integrated SSM that incorporates both primary and secondary controllers to assess the impact of the combined primary and secondary gains on the microgrid domain of stability (DOS) taking into consideration the communication delay produced by secondary control. The secondary control model includes voltage and frequency restoration as well as controlling the RPS. Furthermore, the influence of the secondary controller gains on the microgrid stability is studied using the investigated SSM, considering the influence of the communication delay. Lastly, the effect of the secondary controller gains, the communication delay, the RPS gain on the stability domain

considering the proportional derivative reactive controller are studied. Interesting results regarding the influence of the secondary controller gain on the microgrid stability are obtained. Further, very supportive stability domain charts for RPS and the secondary controller gain are obtained. The stability domain results are verified through repeated dynamic simulations using MATLAB/SIMULINK.

This paper is arranged as follows. In the next section, a complete SSM of the combined secondary and primary control is developed. Model analysis using eigenvalue of the integrated SSM and its influence on the DOS is examined in Section III. Different simulation scenarios to validate the eigenvalue analyses are discussed in Section IV. Conclusions are stated in Section V.

## II. INTEGRATED PRIMARY AND SECONDARY SMALL-SIGNAL MODEL

The integrated SSM incorporating both primary and secondary controllers for islanded microgrids is presented in this section. The developed SSM includes the active power gain and the proportional derivative reactive power droop for the primary control layer, the PI controllers for the frequency and voltage regulation at the secondary control level, the RPS controller and the impact of the communication delay produced by transfer the no-load frequency and voltage to the DGs. The detailed structure of the primary and secondary controllers of the used microgrid is shown in Fig. 1. The microgrid model under consideration has three DGs, as seen in Fig. 1. The active and reactive droop controllers are used to implement the primary controller. The microgrid frequency and the DG voltages must be measured for the secondary controller, which is implemented as a PI controller. The mathematical model for both primary and secondary controllers for inverter-based DG (IBDG) microgrids is presented in the next subsection. The integrated SSM of the overall microgrid is obtained in the following subsections.

### A. PRIMARY CONTROL MODEL

In this subsection, the primary control model incorporating a PD reactive power droop controller for the IBDG discussed in [24] is summarized. The main modifications between the primary controller presented in this paper and the primary controller given in [24] is in introducing two terms in the speed and voltage equations to take into consideration the secondary controller effects. As a result, the updated equations and matrices are developed for the power controller, along with how they affect the overall microgrid model. The complete details of the current controller, voltage controller, power controller and LCL filter are stated in [24] and referred to with the same notation in this paper. The primary control structure is shown in Fig. 2 a.

The power controller objective is to stabilize the operating frequency and voltage of the IBDG microgrid. Traditionally, this can be attained using the active droop gain ($m_P$) and reactive droop gain ($n_q$). In this paper, a PD controller with proportional and derivative gains of ($n_q$) and ($k_d$), respectively, is used instead of the reactive gain. It has been shown in [24] that a PD for reactive power control has a much more profound effect on enhancing the stability margin in comparison to the PD active power control. Therefore, the droop equations can be written as follows.

$$\begin{cases} \omega = \omega_n - m_P P \\ v^*_{od} = V_n - n_q Q - k_d \dfrac{dQ}{dt} \\ v^*_{oq} = 0 \end{cases} \tag{1}$$

where $V_n$, $\omega_n$, $\omega, Q, P$ and $v^*_{odq}$ are the no-load voltage, no-load frequency, operating frequency, reactive power, active power, and the reference output voltage in dq frame, respectively. In the primary layer, the no-load frequency and voltage are constant at the rated values. However, in the secondary layer, the no-load frequency and voltage are varied to keep the operating voltage and frequency at their rated values. In this paper, the droop equations are modified to include the secondary control actions as follows:

$$\begin{cases} \omega = \omega_n + \omega_{ns} - m_P P \\ v^*_{od} = V_n + V_{ns} - n_q Q - k_d \dfrac{dQ}{dt} \\ v^*_{oq} = 0 \end{cases} \tag{2}$$

where $V_{ns}$ and $\omega_{ns}$ are the required modifications in the voltage and frequency produced by the secondary control to operate the microgrid at $V_n$ and $\omega_n$ at steady state, respectively. The droop equations given in (2) are linearized around the operating point as follows:

$$\begin{cases} \Delta\omega = \Delta\omega_{ns} - m_P \Delta P \\ \Delta v^*_{od} = \Delta V_{ns} - n_q \Delta Q - k_d \Delta \dfrac{dQ}{dt} \\ \Delta v^*_{oq} = 0 \end{cases} \tag{3}$$

With the same procedure given in [13] and [24], the SSM of the power controller can be obtained as follow:

$$\begin{cases} \dot{x}_1 = \begin{cases} A_P\,[x_1] + B_P\,[x_2] + B_{Pwcom}\,[\Delta\omega_{com}] \\ +B_{Pwns}\,[\Delta\omega_{ns}] \end{cases} \\ \begin{bmatrix} \Delta\omega \\ \Delta v^*_{odq} \end{bmatrix} = \begin{cases} \begin{bmatrix} C_{Pw} \\ C_{Pv} \end{bmatrix} [x_1] + \begin{bmatrix} D_{Pw} \\ D_{Pv} \end{bmatrix} [x_2] \\ +B_{Pwns}\,[\Delta\omega_{ns}] + B_{Pvns}\,[\Delta V_{ns}] \end{cases} \end{cases} \tag{4}$$

where

$$x_1 = \begin{bmatrix} \Delta\delta \\ \Delta P \\ \Delta Q \end{bmatrix}, \quad x_2 = \begin{bmatrix} \Delta i_{ldq} \\ \Delta v_{odq} \\ \Delta i_{odq} \end{bmatrix}, \quad \mathrm{B_{Pwcom}} = \begin{bmatrix} -1 \\ 0 \\ 0 \end{bmatrix}$$

$$B_{Pwns} = \begin{bmatrix} 1 \\ 0 \\ 0 \end{bmatrix}, B_{Pvns} = \begin{bmatrix} 0 \\ 1 \\ 0 \end{bmatrix}, C_{Pv} = \begin{bmatrix} 0 & 0 & -n_q + \omega_c k_d \\ 0 & 0 & 0 \end{bmatrix}$$

$A_P$, $B_P$, $C_{Pw}$, $D_{Pw}$, and $D_{Pv}$ are defined in [13] and [24].

By combining the modified power control loop equations given in (4), the voltage control loop, the current control loop

and LCL filter, which given in details in [13], the inverter model can be written as follows:

$$\begin{cases} [\Delta\dot{x}_{invi}] = \begin{cases} A_{invi}\,[\Delta x_{invi}] + B_{invi}\,[\Delta v_{bDQi}] \\ +B_{Pwcomi}\,[\Delta\omega_{com}] \\ +B_{Pvnsi}\,[\Delta V_{nsi}] + B_{Pwnsi}\,[\Delta\omega_{nsi}] \end{cases} \\ \begin{bmatrix} \Delta w_i \\ \Delta i_{oDQi} \end{bmatrix} = \begin{cases} \begin{bmatrix} C_{invwi} \\ C_{invci} \end{bmatrix} [\Delta x_{invi}] + + \begin{bmatrix} 1 \\ 0 \end{bmatrix} [\Delta\omega_{nsi}] \\ + \begin{bmatrix} 0 \\ B_{Pvnsl} \end{bmatrix} [\Delta V_{nsi}] \end{cases} \end{cases} \tag{5}$$

where $\Delta x_{invi}$ consists of 13 states and defined as $\Delta x_{invi} = [x_1 \Delta\emptyset_{dqi} \Delta\gamma_{dqi} x_2]^{\mathrm{T}}$. $\dot{\gamma}_{dq} = i^*_{ldq} - i_{ldq}$ and $\dot{\emptyset}_{dq} = V^*_{odq} - V_{odq}$.

$$B_{Pvnsi} = \begin{bmatrix} 0 \\ B_{v1i} B_{Pvnsl} \\ B_{c1i} D_{v1i} B_{Pvnsl} \\ B_{LCL1i} D_{c1i} D_{v1i} B_{Pvnsl} \end{bmatrix}_{1\times 13} B_{Pvnsl} = \begin{bmatrix} 1 \\ 0 \end{bmatrix}_{1\times 2}, \; B_{Pwnsi} = \begin{bmatrix} B_{Pwns} \\ 0 \\ 0 \\ B_{LCL3i} \end{bmatrix}_{1\times 13}.$$

The remaining matrices given in (5) are defined in [13] and [24].

### B. SECONDARY CONTROL MODEL

In this subsection, the effect of the secondary controller on the SSM is discussed. The main target of the secondary control is to produce the change in the no-load variables $\omega_{ns}$ and $V_{ns}$ to fix the microgrid frequency and voltages at their rated values at steady-state and control the RPS. For secondary frequency regulation, a PI controller is designed to keep the signals $(\omega - \omega_n)$ at zero value at steady state. For secondary voltage control, a tradeoff PI controller is designed to either maintain the microgrid voltage or to control the RPS by keeping the signal $(v^*_{odi} - V_n)$ at zero value on steady state as in [22]. The output of these controllers ($\omega_{ns}$ and $V_{nsi}$) are added to the droop equations given in (2). These outputs will be transferred to all DGs with a communication delay of $(\tau)$ which can be represented in the continuous time domain by $\mathrm{e}^{-\tau s}$. The block diagram that describes the secondary controller structure is drawn in Fig. 2b.

The primary control modeling equations given in (5) are in-terms of the secondary control variables $\Delta\omega_{ns}$ and $\Delta V_{ns}$. In order to develop the overall microgrid model, the secondary control modeling equations are formulated based on the block diagram given in Fig. 2b. as follows:

$$\begin{cases} \dot{x}_3 = k_{ws}(\omega_n - \omega) \\ \dot{x}_4 = k_{vs}\left(V_n - v^*_{od1}\right) - k_{qs}(-2Q_1 + Q_2 + Q_3) \\ \dot{x}_5 = k_{vs}\left(V_n - v^*_{od2}\right) - k_{qs}(-2Q_2 + Q_1 + Q_3) \\ \dot{x}_6 = k_{vs}\left(V_n - v^*_{od3}\right) - k_{qs}(-2Q_3 + Q_1 + Q_2) \end{cases} \tag{6}$$

where $k_{qs}$, $k_{ws}$, and $k_{vs}$ are the secondary reactive sharing, frequency, and voltage gains, respectively. As shown in Fig. 2b, the secondary frequency control requires a measurement of the microgrid frequency, which is compared with the reference frequency, and an integrator is used to eliminate the steady state error, followed by the communication network to send the change in the no load frequency. On the other hand, the secondary voltage controller requires the measurements from the DG voltages to regulate the DG voltages or the measurement from the reactive power to improve the RPS. The SSM of the secondary states ($x_3$, $x_4$, $x_5$ and $x_6$) produced by the secondary controller can be written using (3) and (6) as follows:

$$\begin{cases} \Delta\dot{x}_3 = -k_{ws}(\Delta\omega_{ns1} - m_P\Delta P_1) \\ \Delta\dot{x}_4 = \begin{cases} -k_{vs}\Delta V_{ns1} - k_{vs}D_{vs1}x_2 \\ +(k_{vs}n_q - k_{vs}k_d\omega_c - 2k_{qs})\Delta Q_1 \\ +k_{qs}\,(\Delta Q_2 + \Delta Q_3) \end{cases} \\ \Delta\dot{x}_5 = \begin{cases} -k_{vs}\Delta V_{ns2} - k_{vs}D_{vs2}x_2 \\ +(k_{vs}n_q - k_{vs}k_d\omega_c - 2k_{qs})\Delta Q_2 \\ +k_{qs}\,(\Delta Q_1 + \Delta Q_3) \end{cases} \\ \Delta\dot{x}_6 = \begin{cases} -k_{vs}\Delta V_{ns3} - k_{vs}D_{vs3}x_2 \\ +(k_{vs}n_q - k_{vs}k_d\omega_c - 2k_{qs})\Delta Q_3 \\ +k_{qs}\,(\Delta Q_1 + \Delta Q_2) \end{cases} \end{cases} \tag{7}$$

where $D_{vsi} = k_d\omega_c \begin{bmatrix} 0 & 0 & I_{oqi} & -I_{odi} & -V_{oqi} & V_{odi} \end{bmatrix}$ and $i$ is the DG number ($i = 1$ or 2 or 3).

As discussed earlier and shown in Fig. 2b, the output of these PI controllers is transferred to the DGs through a communication network. The communication network mainly represented by $e^{-\tau s}$ ($\tau$ is the communication delay). Hence, the secondary control variables $\Delta\omega_{nsi}$ and $\Delta V_{nsi}$ for all DGs can be written as follows:

$$\begin{cases} \Delta\omega_{nsi} = e^{-\tau s}x_3(s) \\ \Delta V_{ns1} = e^{-\tau s}x_4(s) \\ \Delta V_{ns2} = e^{-\tau s}x_5(s) \\ \Delta V_{ns3} = e^{-\tau s}x_6(s) \end{cases} \tag{8}$$

In the literature, several methods approximate the communication delay in the continuous time domain based on bade plot analysis [25]. The most common approximation used in the literature is based on the Taylor approximation. As given in (9), the communication delay can be approximated by a first-order system that consists of one pole and one zero. Hence, by using this approximation, the secondary modeling equations given in (8) can be rewritten as follows:

$$\begin{cases} \Delta\omega_{nsi} = \dfrac{2-\tau s}{2+\tau s}x_3(s) \\ \Delta V_{ns1} = \dfrac{2-\tau s}{2+\tau s}x_4(s) \\ \Delta V_{ns2} = \dfrac{2-\tau s}{2+\tau s}x_5(s) \\ \Delta V_{ns3} = \dfrac{2-\tau s}{2+\tau s}x_6(s) \end{cases} \tag{9}$$

By converting the secondary communication delay equations given in (9) into time domain equations using Laplace inverse, this leads to:

$$\begin{cases} \Delta\dot{\omega}_{nsi} = \frac{2}{\tau}x_3 - \frac{2}{\tau}\Delta\omega_{nsi} - \Delta\dot{x}_3 \\ \Delta\dot{V}_{ns1} = \frac{2}{\tau}x_4 - \frac{2}{\tau}\Delta V_{ns1} - \Delta\dot{x}_4 \\ \Delta\dot{V}_{ns2} = \frac{2}{\tau}x_5 - \frac{2}{\tau}\Delta V_{ns2} - \Delta\dot{x}_5 \\ \Delta\dot{V}_{ns3} = \frac{2}{\tau}x_6 - \frac{2}{\tau}\Delta V_{ns3} - \Delta\dot{x}_6 \end{cases} \tag{10}$$

By substituting (7) into (10), the secondary control time domain equations can be written as:

$$\begin{cases} \Delta\dot{\omega}_{nsi} = \begin{cases} \frac{2}{\tau}x_3 - \frac{2}{\tau}\Delta\omega_{nsi} \\ +k_{ws}(\Delta\omega_{ns1} - m_P\Delta P_1) \end{cases} \\ \Delta\dot{V}_{ns1} = \begin{cases} \frac{2}{\tau}x_4 + (k_{vs} - \frac{2}{\tau})\Delta V_{ns1} \\ -k_{qs}\Delta Q_2 - k_{qs}\Delta Q_3 + k_{vs}D_{vs1}x_2 \\ -(k_{vs}n_q - k_{vs}k_d\omega_c - 2k_{qs})\Delta Q_1 \end{cases} \\ \Delta\dot{V}_{ns2} = \begin{cases} \frac{2}{\tau}x_5 + (k_{vs} - \frac{2}{\tau})\Delta V_{ns2} \\ -k_{qs}\Delta Q_1 - k_{qs}\Delta Q_3 + k_{vs}D_{vs2}x_2 \\ -(k_{vs}n_q - k_{vs}k_d\omega_c - 2k_{qs})\Delta Q_2 \end{cases} \\ \Delta\dot{V}_{ns3} \begin{cases} \frac{2}{\tau}x_6 + (k_{vs} - \frac{2}{\tau})\Delta V_{ns3} \\ -k_{qs}\Delta Q_1 - k_{qs}\Delta Q_2 + k_{vs}D_{vs3}x_2 \\ -(k_{vs}n_q - k_{vs}k_d\omega_c - 2k_{qs})\Delta Q_3 \end{cases} \end{cases} \tag{11}$$

### C. COMBINED PRIMARY AND SECONDARY MODELS

In order to obtain the complete model of the inverter, the SSM given in (5) is combined with the secondary control SSM given in (7) and 11). As discussed in subsection II-A, each DG has 13 states. From the analysis provided in subsection II-B, the overall microgrid states are increased by ten states. Hence, the three distributed generators in the microgrid under study contain 49 states. The overall inverter model can be written as follows:

$$\begin{cases} [\Delta\dot{x}_{INV}] = A_{INV}\,[\Delta x_{INV}] + B_{INV}\left[\Delta v_{bDQ}\right] \\ \left[\Delta i_{oDQ}\right] = C_{INVc}\,[\Delta x_{INV}] \end{cases} \tag{12}$$

where the matrices used in **(12)** are defined in the appendix.

### D. COMPLETE MICROGRID MODEL

The complete SSM of the microgrid can be written by modeling the microgrid network and load. For brevity, the complete details for modeling the network and load are given in [13]. The differential equations of the load ($\Delta i_{LoadDQ}$) and network ($\Delta i_{lineDQ}$) currents in the $dq$ frame can be written as follows:

$$\begin{cases} \Delta\dot{i}_{lineDQ} = \mathrm{A_{NET}}\Delta i_{lineDQ} + \mathrm{B_{1NET}}\Delta v_{bDQ} \\ \quad +\mathrm{B_{2NET}}\Delta\omega \\ \Delta\dot{i}_{loadDQ} = \mathrm{A_{Load}}\Delta i_{LoadDQ} + \mathrm{B_{1Load}}\Delta v_{bDQ} \\ \quad +\mathrm{B_{2Load}}\Delta\omega \end{cases} \tag{13}$$

where $\Delta\omega = \Delta\omega_{com}$, $\mathrm{B_{1NET}}$, $\mathrm{B_{2NET}}$, $\mathrm{A_{NET}}$, $\mathrm{A_{Load}}$, $\mathrm{B_{1Load}}$, and $\mathrm{B_{2Load}}$ are the network mode matrices and defined in [13]. The SSM of the bus voltage can be written as follows:

$$\Delta v_{bDQ} = R_N\left\{M_{INV}\Delta i_{oDQ} + M_{Load}\Delta i_{loadDQ} + M_{Net}\Delta i_{ineDQ}\right\} \tag{14}$$

where the matrices $\mathrm{M_{Load}}$, and $\mathrm{M_{Net}}$, $\mathrm{M_{INV}}$ map the loads, lines, and the DGs connection points to the nodes, respectively. $\mathrm{R_N}$ is a large virtual resistance. The complete microgrid model can be written by combining the SSM given in (12), (13) and (14).

$$\begin{bmatrix} \Delta\dot{x}_{INV} \\ \Delta i_{lineDQ} \\ \Delta i_{loadDQ} \end{bmatrix} = A_{MG}\begin{bmatrix} \Delta x_{INV} \\ \Delta i_{lineDQ} \\ \Delta i_{loadDQ} \end{bmatrix} \tag{15}$$

For brevity, the matrices $\mathrm{M_{INV}}$, $\mathrm{M_{Net}}$, and $\mathrm{M_{Load}}$ are provided as in [13]. The complete microgrid matrix $\mathrm{A_{MG}}$ is constructed as given in [13] with the modified inverter SSM given in (12).

## III. EIGENVALUE STABILITY ANALYSIS

In this section, the proposed integrated SSM is assessed based on the eigenvalues analysis considering various cases to assess influence of secondary controller gains on the microgrid DOS. The first case represents the benchmark case where the DOS is obtained considering only primary control. The second case study analyzes the influence of the secondary control gains of the microgrid DOS, considering only frequency and voltage regulation as the only available control actions. The third case study examines the effect of equal RPS as a secondary control measure on microgrid stability. The last case study analyzes the effect of the communication delay on the microgrid performance and stability. The controller parameters used for stability analysis in the aforementioned cases are summarized in Table 1. These cases are performed for the IBDG model plotted in Fig. 1 with the parameters presented in Table 2. Further, the eigenvalues analysis is based on the SSM given in (15) and verified using a SIMULINK/MATLAB model.

### A. BENCHMARK CASE WITH PRIMARY CONTROL ONLY

As mentioned earlier, the primary control is designed such that active power controller is equipped with a proportional gain while a PD controller is implemented for the reactive power controller. In this case study, both transient and stability analyses are assessed considering only primary control, representing the base case. From the SSM analysis, the influence of the derivative gain on the dominant pole

**TABLE 1. Controller parameters used for stability analysis for all cases.**

| Cases | $m_p$ range | $k_d$ | $k_{vs}, k_{\omega s}$ | $k_{qs}$ | $\tau$ |
|---|---|---|---|---|---|
| III.A | $1.9\times10^{-6}$ - $11.5\times10^{-4}$ | 0,5 × $10^{-5}, 10^{-4}$ | 0 | 0 | 0 |
| III.B | $1.9\times10^{-6}$ – $81\times10^{-4}$ | $10^{-4}$ | 0, 50, 100 | 0 | 0.02 |
| III.C | $1.9\times10^{-6}$ – $81\times10^{-4}$ | $10^{-4}$ | $k_{\omega s}$ =50 $k_{vs}$ =0 | 0,0.2 ,0.4 | 0.02 |
| III.D | $1.9e^{-6}$ - $8e^{-4}$ | $10^{-4}$ | 5 | 0 | 0.02, 0.1, 0.3, 0.4 |

**TABLE 2. Parameters of microgrid under investigation.**

| Parameter | Value | Parameter | Value |
|---|---|---|---|
| $R_C$ | 0.03 | $L_{load1}, L_{load2}$ | 0.1e-1 |
| $L_C$ | 0.35e-3 | $R_{load1}, R_{load2}$ | 25 |
| $C_f$ | 50e-6 | $w_c$ | 31.41 |
| $R_f$ | 0.1 | $F$ | 0.75 |
| $L_f$ | 1.35e-3 | $k_{pc}$ | 10.5 |
| $R_{line2}$ | 0.35 | $k_{ic}$ | 16e3 |
| $L_{ine2}$ | 1.85e-3 | $k_{iv}$ | 390 |
| $R_{line1}$ | 0.23 | $k_{pv}$ | 0.05 |
| $L_{line1}$ | 0.35e-3 | | |

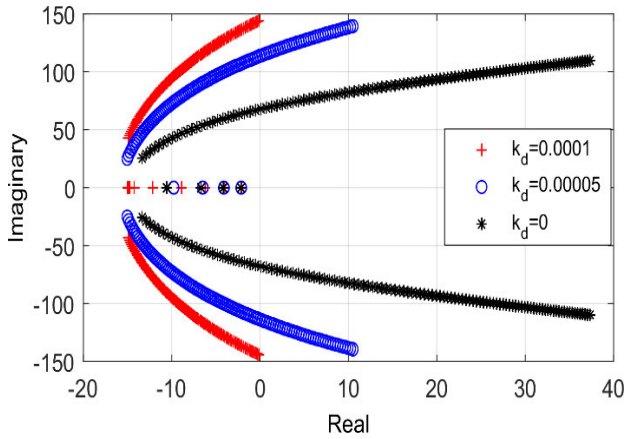


**FIGURE 3. Dominant pole variations with $k_d$.**

location as $m_p$ varies from $1.9\times10^{-6}$ to $11.5\times10^{-4}$ at constant $n_q$ ($1.3\times10^{-3}$) is shown in Fig. 3. It is shown that the dominant pole location approaches *jw* axis faster when the derivative gain $k_d = 0$ (no derivative term). Increasing the derivative gain to $10^{-4}$ moves the dominant pole far from the jw axis toward the LHS, which improves the microgrid transient performance.

The stability domain chart in Fig. 4 shows the maximum allowable active power droop (max. $m_p$) at different values of the reactive power droop gain ($n_q$) for $k_d = 0, 5\times10^{-5}$ and $10^{-4}$. All combinations of ($n_q$, $m_p$) within the stability domain chart ensure microgrid stabile operation. As shown in Fig. 4, the stability domain increases significantly when using the derivative gain in the reactive power droop and thus, if considering only primary control, the PD reactive

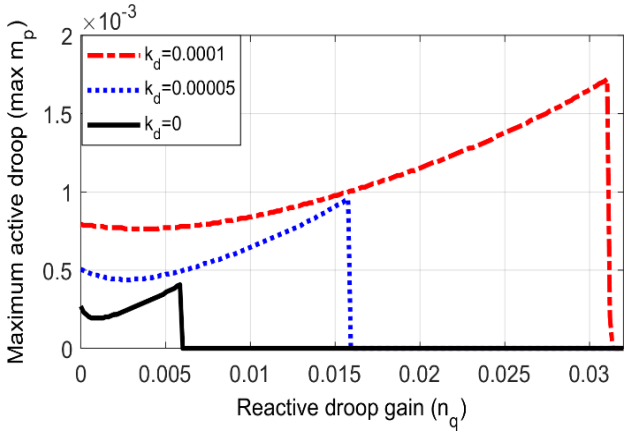


**FIGURE 4. DOS at different $k_d$.**

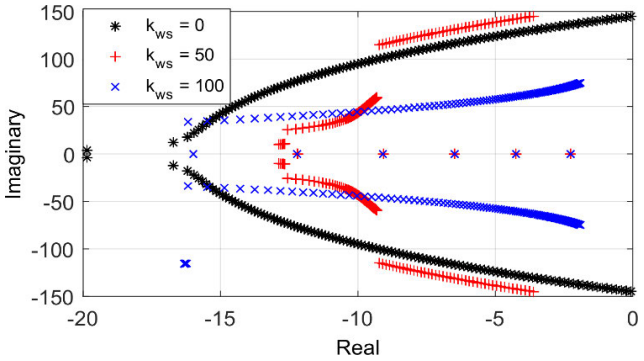


**FIGURE 5. Dominant pole variations with secondary control gains.**

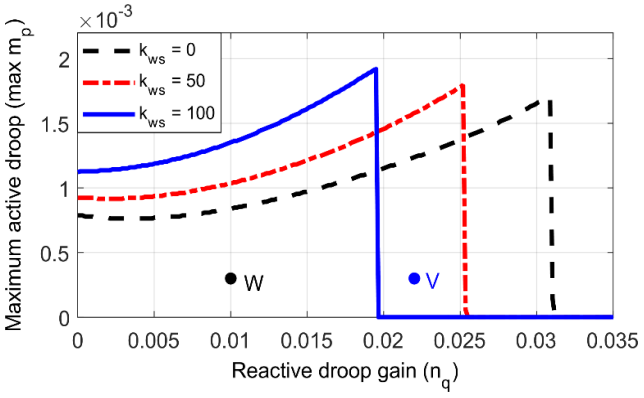


**FIGURE 6. DOS for different secondary control gains.**

power droop with a derivative gain of $k_d = 10^{-4}$ would be the best option. The stability domain chart, given in Fig. 4, corresponding to primary control with $k_d = 10^{-4}$, will be used as the base case for the comparative analysis presented in the next subsections.

The DOS chart and eigenvalue analysis presented in Fig. 4 and Fig. 3, respectively, confirm the fact of the PD controller for enhancing transient performance. This is achieved by moving the system's eigenvalue towards the LHS of the jw axis.

### B. SECONDARY CONTROL WITH VOLTAGE AND FREQUENCY REGULATION

To assess the impact of the secondary controller gains on the stability domain, the variations in the dominant pole location and the stability domain chart are plotted in Fig. 5 and Fig. 6, respectively. The integrated primary and secondary control model proposed in the previous section is implemented. The analyses are carried out with a communication delay ($\tau$) of 20 msec. The frequency secondary gain ($k_{\omega s}$) and voltage secondary gain ($k_{vs}$) are both set to the same value. Fig. 5 depicts the variation of the dominant pole location when $m_p$ varies from $1.91 \times 0^{-6}$ to $81 \times 0^{-4}$. As shown in Fig. 5, the effect of three different secondary gains is studied at a constant $n_q$ of $1.3e^{-3}$, and the RPS is disabled. It is worthy to note that, at $m_p = 8{\times}10^{-4}$, the dominant pole is placed on the *jw* axis when the secondary gains are equal to zero (no secondary control is included). Furthermore, for the same active power droop, a better dominant pole location is achieved using a secondary control gain of 50. Hence, Fig. 5 shows that the secondary gains significantly affect the dominant pole location and, therefore, the microgrid's transient performance. To elaborate further, Fig. 6 shows the stability domain chart considering different secondary controller gains. As shown in Fig. 6, the secondary controller gains directly affect the stability domain of the microgrid. Increasing the secondary control gain affects the primary control operating region (dotted black line). Hence, the selection of the secondary gains in combination with the primary gains is very important for the better and more robust operation of microgrids.

### C. IMPACT OF REACTIVE POWER SHARING GAIN ON MICROGRID STABILITY

In this case study, the secondary control is designed to provide frequency regulation and RPS. The influence of the reactive RPS gain ($k_{qs}$) on the microgrid stability is presented in Fig. 7. As seen from the stability domain chart, it significantly affects microgrid stability. It is also noted that the RPS gain moves the DOS curve right and thus narrowing the operating region for the primary control reactive power droop gain. This means that in order to maintain the microgrid stability with RPS improvement, the reactive power droop gain ($n_q$) should be increased to be within the stable operating region. Thus, the selection of $n_q$ is critical for maintaining stable operation with RPS.

Furthermore, the influence of the RPS gain on the dominant pole location is analyzed. The variation of the dominant pole for the operating points on line A, shown in Fig. 7, is plotted in Fig. 8. For $k_{qs} = 0$, the dominant pole of all operating points on line A is located in the LHS of the *jw* axis. Further, for $k_{qs} = 0.2$, some of the operating points is unstable. Furthermore, for $k_{qs} = 0.4$, all the operating points of line A are unstable. These analyses verify the stability domain chart shown in Fig. 7.

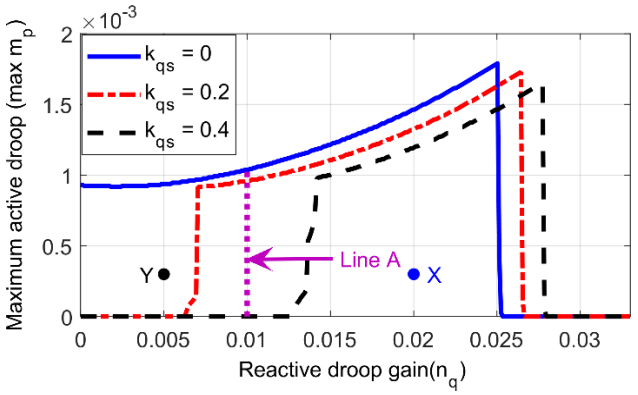


**FIGURE 7.** DOS at different RPS gains at $k_{\omega s} = 50$.

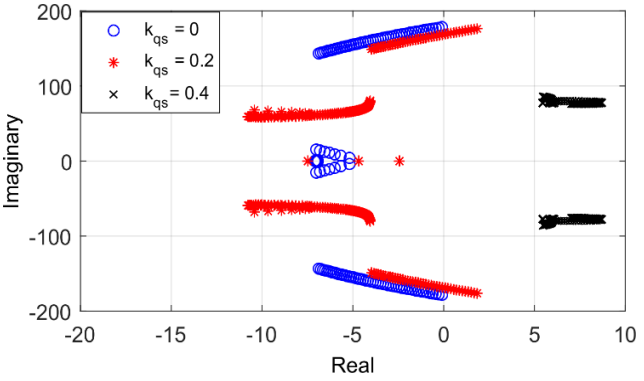


**FIGURE 8.** Dominant pole variations with RPS gains.

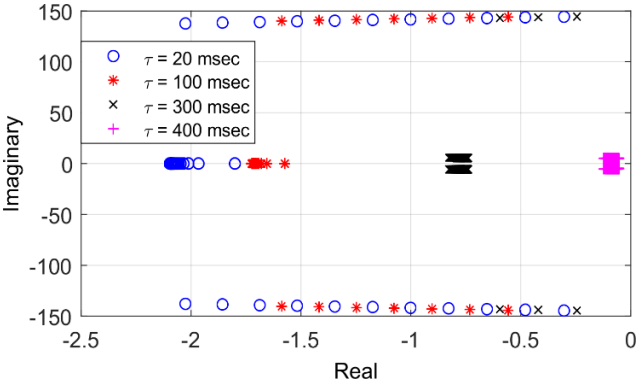


**FIGURE 9.** Dominant pole variations with communication delay at $k_{\omega s} = k_{vs} = 5$.

### D. IMPACT OF TIME DELAY ON MICROGRID STABILITY

Communication delay between the central unit and DGs is one of the main factors that could affect microgrid stability. The impact on the dominant pole location and stability domain chart for different communication delays are presented in this subsection. Fig. 9 shows the variations of the dominant pole with four different communication time delay ($\tau$). The analysis is performed at $k_{\omega s} = k_{vs} = 5$, $k_{qs} = 0$, $n_q = 1.3e^{-3}$. As shown in Fig. 9, the dominant pole location is in the LHS of the jw axis for a communication

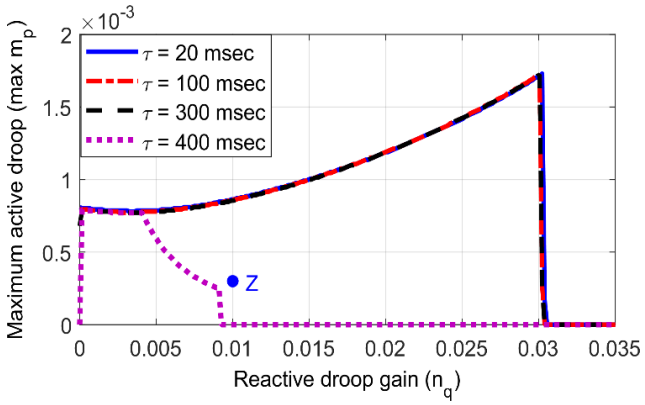


**FIGURE 10.** DOS for different communication delay at $k_{\omega s} = k_{vs} = 5$.

delay of 20 msec., 100 msec., 300 msec. and 400 msec. for $m_p$ ranging from $1.9e^{-6}$ to $8e^{-4}$. It is shown that for a communication delay of up to 400 msec., the microgrid maintains stable operation for the same maximum active power droop ($m_p = 8e^{-4}$). However, better transient performance can be achieved by decreasing the communication delay as the dominant pole moves toward the jw axis by increasing the communication delay. Hence, higher communication delay leads to reduced transient performance and results in a reduction in the DOS. The DOS charts that support the analyses of the dominant pole variations are shown in Fig. 10. It is also noted that decreasing the secondary gains maintains the microgrid stability with higher communication delay and vice versa.

It is also noted that the obtained results confirmed two control facts. The first fact is that higher communication delays lead to poor performance. The second fact is that in order to maintain the system's stability with higher communication delays, a control action needs to be non-aggressive, which can be achieved by reducing the controller gain.

## IV. SIMULATION RESULTS

Simulation results are performed to validate the eigenvalue analyses of the two-level controllers discussed in section III. Three simulation scenarios are tested. In the first case study, the impact of the secondary controller gains for frequency and voltage regulation on microgrid DOS is analyzed. In the second case study, the impact of equal RPS through secondary control is simulated and verified against the results presented in section III. In the third case study, the influence of secondary controller communication delays on the microgrid DOS is discussed.

### A. SECONDARY CONTROLLER WITH FREQUENCY AND VOLTAGE REGULATION

In this study, the impact of the secondary controller on the microgrid DOS is analyzed. For this case study, the secondary controller is designed to perform frequency regulation and voltage regulation. Two different operating points

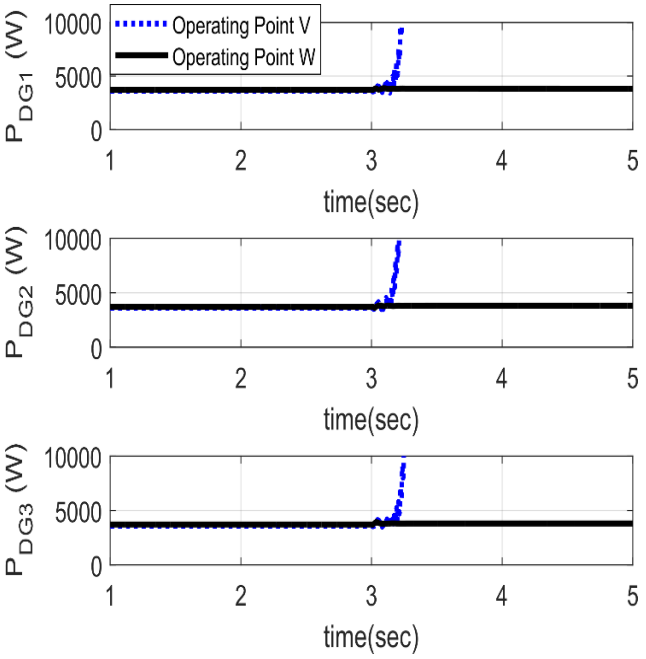


**FIGURE 11.** Active power of the three DGs for operating points V and W.

(W and V) shown in Fig. 6 are considered for the same secondary controller gains ($k_{\omega s} = k_{vs} = 100$) and $\tau = 20$ msec. The main difference between the two operating points is the value of reactive droop gain ($n_q$). In this test, the microgrid operates with primary control only for the first 3 seconds. The secondary controller is activated at t = 3 sec. The active power sharing response is shown in Fig. 11. Prior to activating the secondary controller, both points W and V result in a stable operating condition. Once the secondary controller is activated, the results show that the operating point W maintains the microgrid stability while the operating point V leads to instability. Further, the microgrid frequency and bus voltages of the operating point W are shown in Fig. 12 and Fig. 13, respectively. As seen from these figures, the secondary controller maintains the microgrid frequency and voltages at their rated values. The results coincide with the stability domain chart shown in Fig. 6 and highlight the influence of the secondary control gains of the microgrid DOS. For secondary control with frequency and voltage regulation, higher value of reactive power droop gain can lead to microgrid instability.

### B. SECONDARY CONTROL WITH REACTIVE POWER SHARING

In order to validate the impact of the RPS controller gain on the microgrid DOS, the performance of the proposed controller is verified at $k_{qs} = 0.2$ for two different operating points (X and Y) shown in Fig. 7. The two operating points have the same parameters except for the reactive power droop gain. In this test, the microgrid operates with the secondary controller performing both frequency and voltage regulation for the first 2 seconds. The RPS is activated at t = 3 sec. Based

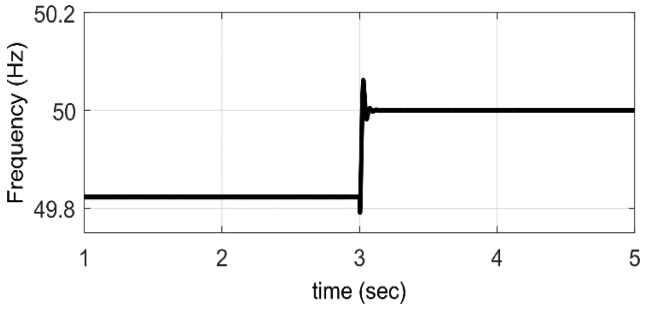


**FIGURE 12.** Microgrid frequency for operating point W.

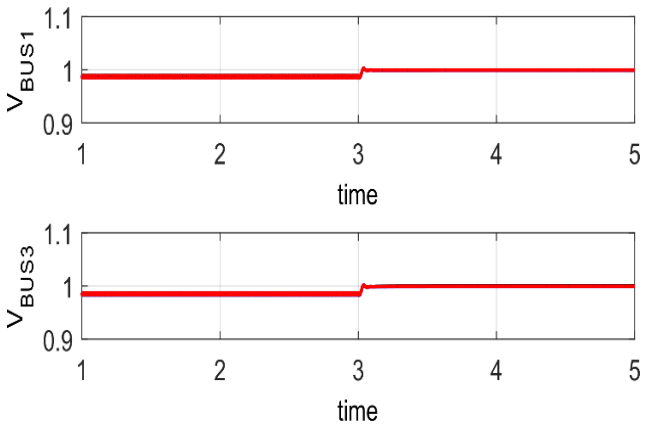


**FIGURE 13.** Three phase buses voltages for operating point W.

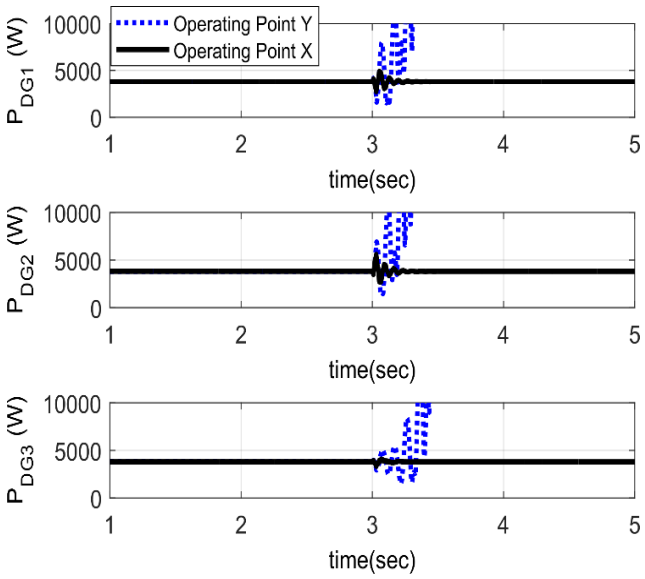


**FIGURE 14.** Active power-sharing of the three DGs for operating points X and Y.

on the stability domain chart shown in Fig. 7, the operating point X is stable while the operating point Y is unstable. The active power sharing responses of the two operating points are shown in Fig. 14. The RPS results coincide with the results obtained from the stability domain chart shown in Fig. 7. Further, the RPS response for the stable operating point

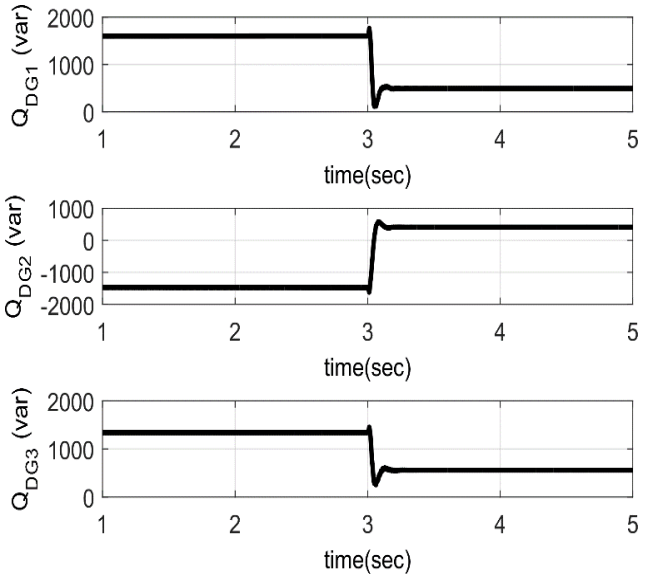


**FIGURE 15.** RPS of the three DGs for operating point X.

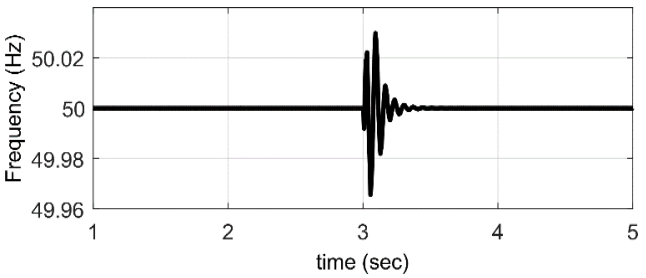


**FIGURE 16.** Microgrid frequency for operating point X.

X is shown in Fig. 15. As seen from Fig. 15, for the first 2 secs., the DGs are sharing the reactive power unequally while both the frequency and voltage are regulated, as seen in Fig. 16 and Fig. 17. However, after activating the RPS "gain ($k_{qs}$)", the three DGs are supplying approximately the same reactive power. Further, the microgrid frequency is kept at the rated value irrespective of the activation of the RPS controller, as shown in Fig. 16. However, the bus voltages are slightly different, as shown in Fig. 17. The results show that a secondary controller with RPS can adversely affect the microgrid stability. Contrary to the previous case, lower reactive power droop gains can lead to microgrid instability. In general, the results show that secondary control design can significantly impact the microgrid stability and the DOS serves as a advantageous tool for recognizing the best combination of primary and secondary gains to achieve stable operation.

### C. IMPACT OF COMMUNICATION DELAY

For this case study, the impact of communication delay on microgrid stability and the design of the primary and secondary controller are investigated. The primary control gains correspond to Point Z in Fig. 10. The secondary controller gains are set at $k_{vs} = k_{\omega s} = 5$ and communication

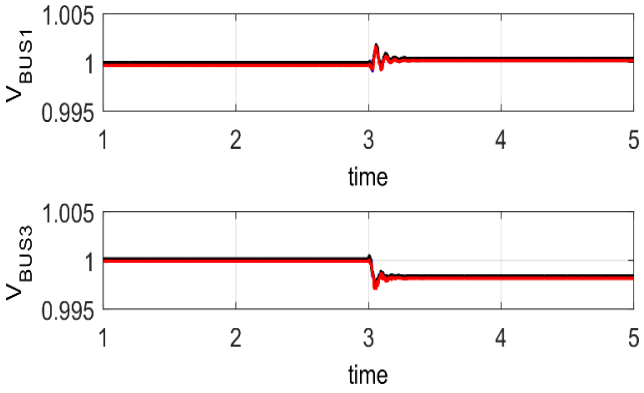


**FIGURE 17.** Buses voltages for operating point X.

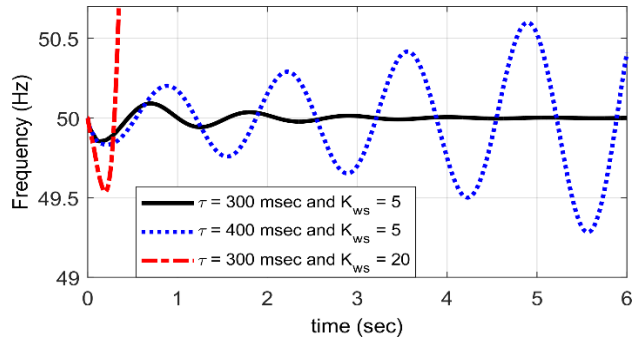


**FIGURE 18.** Microgrid frequency for operating point Z considering different communication delays and secondary controller gains.

delay values of 0.3 and 0.4 sec are considered to examine the impact of communication delay on microgrid stability. From brevity, Fig. 18 presents the microgrid-grid frequency for the two aforementioned communication delays. As can be seen, a higher communication delay can affect the microgrid stability, and the results coincide with the DOS chart presented in Fig. 10. An additional case is simulated and presented in Fig. 18 where a higher secondary gain of $k_{vs} = k_{\omega s} = 20$ is utilized considering a communication delay of 0.3 sec. As shown in Fig. 18, for the same communication delay of 0.3 sec, the lower secondary controller gain of $k_{\omega s} = 5$ maintains the microgrid while a higher secondary gain of $k_{\omega s} = 20$ can result in microgrid unstable operation. Therefore, to maintain the microgrid stability at higher communication delay, the secondary controller gains should be reduced.

The results show that the DOS chart can serve as a helpful tool for deciding the best combination of primary and secondary gains while considering communication delays. Table 3 provides a summary of the simulation scenarios. Two operating points are chosen to be examined for each simulation scenario, as illustrated in Table 3. The first operating point for each of the three scenarios (W, X and Z at $\tau = 300$) is chosen to be inside the associated DOS. The results showed that the microgrid was stable at these operating points. Nevertheless, the second operational point (V, Y and Z at $\tau = 400$) is chosen to be outside the corresponding DOS, causing the microgrid to become unstable.

**TABLE 3.** Summary of the three simulation scenarios.

| Case | | Operating point | DOS | Performance |
|---|---|---|---|---|
| IV.A | Frequency and voltage | W | Inside | Stable |
| | | V | Outside | Unstable |
| IV.B | RPS | X | Inside | Stable |
| | | Y | Outside | Unstable |
| IV.C | Communication delay | Z ( $\tau = 300$) | Inside | Stable |
| | | Z ( $\tau = 400$) | Outside | Unstable |

## V. CONCLUSION

This paper proposes a small signal model that considers the influence of the secondary controller gains, the communication delay, active power droop gain, reactive power droop gain, and reactive power-sharing. The proposed model is used to evaluate the influence of the secondary controller gains, reactive power-sharing, and communication delay on the microgrid domain of stability. The results show that secondary controller gains can adversely impact the microgrid stability and, more significantly, the primary reactive power control. The extent of the impact of secondary control on the microgrid domain of stability will also depend on the secondary control objective. It has been shown that secondary control with the objective of providing reactive power sharing can lead to instability with low primary control reactive power gains. Furthermore, the impact of secondary control can be minimized by reducing secondary control controller gains. The domain of stability chart can provide a useful tool for designing both primary and secondary control while considering communication delays.

## APPENDIX

The matrices stated in equation (12) are defined as:

$$B_{INV} = \begin{bmatrix} B_{inv1} & 0 & 0 \\ 0 & 0 & 0 \\ 0 & B_{inv2} & 0 \\ 0 & 0 & 0 \\ 0 & 0 & B_{inv3} \\ 0 & 0 & 0 \\ 0 & 0 & 0 \\ 0 & 0 & 0 \\ 0 & 0 & 0 \end{bmatrix}_{49\times 6},$$

$$[\Delta v_{bDQ}] = \begin{bmatrix} \Delta v_{bDQ1} \\ \Delta v_{bDQ2} \\ \Delta v_{bDQ3} \end{bmatrix},$$

$$A_{INV} = \begin{bmatrix} A_{11} & 0 & 0 & A_{14} \\ A_{21} & A_{22} & A_{23} & A_{24} \\ A_{31} & A_{32} & A_{33} & A_{34} \\ A_{41} & A_{42} & A_{43} & 0 \end{bmatrix}_{49\times 49},$$

$$A_{21} = \begin{bmatrix} B_{Pwcom2}C_{invw1} & B_{Pwcom2} & 0 \\ -A_{\omega s} & k_{\omega s} & 0 \\ -A_{qs} & 0 & 0 \end{bmatrix},$$

$$A_{11} = \begin{bmatrix} A_{inv1} + B_{Pwcom1} C_{invw1} & B_{Pwcom1} + B_{Pwns1} & B_{Pvns1} \\ -A_{\omega s} & k_{ws} - 2/\tau & 0 \\ -A_{vs} & 0 & k_{vs} - 2/\tau \end{bmatrix}$$

$$A_{invi} = \begin{bmatrix} A_{Pi} & 0 & 0 & B_{Pi} \\ B_{v1i} C_{Pvi} & 0 & 0 & B_{v2i} + B_{v1i} D_{Pvi} \\ B_{c1i} D_{v1i} C_{Pvi} & B_{c1i} C_{vi} & 0 & B_{c1i} D_{v2i} + B_{c2i} + B_{c1i} D_{v1i} D_{Pvi} \\ B_{LCL1i} D_{c1i} D_{v1i} C_{Pvi} + B_{LCL3i} C_{Pwi} & B_{LCL1i} D_{c1i} C_{vi} & B_{LCL1i} C_{ci} & A_{LCLi} + B_{LCL1i} D_{c1i} D_{v2i} + B_{LCL1i} D_{c2i} \\ + B_{LCL2i} \begin{bmatrix} T_{vi}^{-1} & 0 & 0 \end{bmatrix} & & & + B_{LCL3i} D_{Pwi} + B_{LCL1i} D_{c1i} D_{v1i} D_{Pvi} \end{bmatrix}_{13\times 13}$$

$$\Delta x_{INV} = \begin{bmatrix} \Delta x_{inv1} & \Delta \omega_{ns1} & \Delta V_{ns1} & \Delta x_{inv2} & \Delta \omega_{ns2} & \Delta V_{ns2} & \Delta x_{inv3} & \Delta \omega_{ns3} & \Delta V_{ns3} & \Delta x_3 & \Delta x_4 & \Delta x_5 & \Delta x_6 \end{bmatrix}^T_{1\times 49}$$

$$C_{INVc} = \begin{bmatrix} C_{invc1} & 0 & B_{Pvnsl} & 0 & 0 & 0 & 0 & 0 & 0 & 0 & 0 & 0 & 0 \\ 0 & 0 & 0 & C_{invc2} & 0 & B_{Pvnsl} & 0 & 0 & 0 & 0 & 0 & 0 & 0 \\ 0 & 0 & 0 & 0 & 0 & 0 & C_{invc3} & 0 & B_{Pvnsl} & 0 & 0 & 0 & 0 \end{bmatrix}_{6\times 49}$$

$$A_{vs} = \begin{bmatrix} 0 & 0 & \left(k_{vs} n_q - k_{vs} k_d \omega_c - 2k_{qs}\right) & 0 & \dots & 0 & -k_{vs} D_{vs} \end{bmatrix}_{1\times 13}$$

$$A_{22} = \begin{bmatrix} A_{inv2} & B_{Pwns2} & B_{Pvns2} \\ 0 & -\frac{2}{\tau} & 0 \\ -A_{vs} & 0 & k_{vs} - \frac{2}{\tau} \end{bmatrix},$$

$$A_{14} = \begin{bmatrix} 0 & 0 & 0 & 0 \\ \frac{2}{\tau} & 0 & 0 & 0 \\ 0 & \frac{2}{\tau} & 0 & 0 \end{bmatrix},$$

$$A_{23} = A_{32} = \begin{bmatrix} 0 & 0 & 0 \\ 0 & 0 & 0 \\ -A_{qs} & 0 & 0 \end{bmatrix},$$

$$A_{24} = \begin{bmatrix} 0 & 0 & 0 & 0 \\ 2/\tau & 0 & 0 & 0 \\ 0 & 0 & 2/\tau & 0 \end{bmatrix},$$

$$A_{43} = \begin{bmatrix} 0 & 0 & 0 \\ A_{qs} & 0 & 0 \\ A_{qs} & 0 & 0 \\ A_{vs} & 0 & -k_{vs} \end{bmatrix},$$

$$A_{31} = \begin{bmatrix} B_{Pwcom3} C_{invw1} & B_{Pwcom3} & 0 \\ -A_{\omega s} & k_{\omega s} & 0 \\ -A_{qs} & 0 & 0 \end{bmatrix},$$

$$A_{33} = \begin{bmatrix} A_{inv3} & B_{Pwns3} & B_{Pvns3} \\ 0 & -2/\tau & 0 \\ -A_{vs} & 0 & k_{vs} - 2/\tau \end{bmatrix},$$

$$A_{34} = \begin{bmatrix} 0 & 0 & 0 & 0 \\ 2/\tau & 0 & 0 & 0 \\ 0 & 0 & 0 & 2/\tau \end{bmatrix},$$

$$A_{41} = \begin{bmatrix} A_{\omega s} & -k_{ws} & 0 \\ A_{vs} & 0 & -k_{vs} \\ A_{qs} & 0 & 0 \\ A_{qs} & 0 & 0 \end{bmatrix},$$

$$A_{42} = \begin{bmatrix} 0 & 0 & 0 \\ A_{qs} & 0 & 0 \\ A_{vs} & 0 & -k_{vs} \\ A_{qs} & 0 & 0 \end{bmatrix},$$

$$A_{qs} = \begin{bmatrix} 0 & 0 & k_{qs} & 0 & \dots & 0 \end{bmatrix}_{1\times 13}$$

$$A_{\omega s} = \begin{bmatrix} 0 & k_{\omega s} m_P & 0 & \dots & 0 \end{bmatrix}_{1\times 13}$$

## REFERENCES


[1] J. Hu, "Model predictive control of microgrids—An overview," *Renew. Sustain. Energy Rev.*, vol. 136, pp. 1–12, Feb. 2021.

[2] A. A. Eajal, A. H. Yazdavar, E. F. El-Saadany, and M. M. A. Salama, "Optimizing the droop characteristics of AC/DC hybrid microgrids for precise power sharing," *IEEE Syst. J.*, vol. 15, no. 1, pp. 560–569, Mar. 2021.

[3] C. Schwaegerl and L. Tao, "The microgrids concept," in *Microgrids: Architectures Control*, N. Hatziargyriou, Ed. Chichester, U.K.: Wiley, Dec. 2013, ch. 1, pp. 1–24.

[4] A. Bani-Ahmed, M. Rashidi, A. Nasiri, and H. Hosseini, "Reliability analysis of a decentralized microgrid control architecture," *IEEE Trans. Smart Grid*, vol. 10, no. 4, pp. 3910–3918, Jul. 2019.

[5] A. K. Venkatesan, U. Subramaniam, M. S. Bhaskar, O. V. G. Swathika, S. Padmanaban, D. J. Almakhles, and M. Mitolo, "Small-signal stability analysis for microgrids under uncertainty using MALANN control technique," *IEEE Syst. J.*, vol. 15, no. 3, pp. 3797–3807, Sep. 2021.

[6] A. Abhishek, A. Ranjan, S. Devassy, B. K. Verma, S. K. Ram, and A. K. Dhakar, "Review of hierarchical control strategies for DC microgrid," *IET Renew. Power Gener.*, vol. 14, no. 10, pp. 1631–1640, Jul. 2020.

[7] Y. Shan, J. Hu, and J. M. Guerrero, "A model predictive power control method for PV and energy storage systems with voltage support capability," *IEEE Trans. Smart Grid*, vol. 11, no. 2, pp. 1018–1029, Mar. 2020.

[8] D. Y. Yamashita, I. Vechiu, and J. P. Gaubert, "A review of hierarchical control for building microgrids," *Renew. Sustain. Energy Rev.*, vol. 118, pp. 1–18, Feb. 2020.

[9] X. Wu, C. Shen, and R. Iravani, "Feasible range and optimal value of the virtual impedance for droop-based control of microgrids," *IEEE Trans. Smart Grid*, vol. 8, no. 3, pp. 1242–1251, May 2017.

[10] D. E. Olivares, "Trends in microgrid control," *IEEE Trans. Smart Grid*, vol. 5, no. 4, pp. 1905–1919, Jul. 2014.

[11] E. S. N. Raju P. and T. Jain, "A two-level hierarchical controller to enhance stability and dynamic performance of islanded inverter-based microgrids with static and dynamic loads," *IEEE Trans. Ind. Informat.*, vol. 15, no. 5, pp. 2786–2797, May 2019.

[12] X. Wu, Y. Xu, J. He, C. Shen, G. Chen, J. C. Vasquez, and J. M. Guerrero, "Delay-dependent small-signal stability analysis and compensation method for distributed secondary control of microgrids," *IEEE Access*, vol. 7, pp. 170919–170935, 2019.

[13] N. Pogaku, M. Prodanovic, and T. C. Green, "Modeling, analysis and testing of autonomous operation of an inverter-based microgrid," *IEEE Trans. Power Electron.*, vol. 22, no. 2, pp. 613–625, Mar. 2007.

[14] A. Aderibole, H. H. Zeineldin, M. S. El-Moursi, J. C.-H. Peng, and M. Al Hosani, "Domain of stability characterization for hybrid microgrids considering different power sharing conditions," *IEEE Trans. Energy Convers.*, vol. 33, no. 1, pp. 312–323, Mar. 2018.

[15] G. Raman and J. C.-H. Peng, "Mitigating stability issues due to line dynamics in droop-controlled multi-inverter systems," *IEEE Trans. Power Syst.*, vol. 35, no. 3, pp. 2082–2092, May 2020.

[16] D. Dheer, O. Kulkarni, and S. Doolla, "Improvement of stability margin of droop-based islanded microgrids by cascading of lead compensators," *IEEE Trans. Ind. Appl.*, vol. 55, no. 3, pp. 1–10, Feb. 2019.
[17] Y. Mohamed and E. F. El-Saadany, "Adaptive decentralized droop controller to preserve power sharing stability of paralleled inverters in distributed generation microgrids," *IEEE Trans. Power Electron.*, vol. 23, no. 6, pp. 2806–2816, Nov. 2008.
[18] T. Qian, Y. Liu, W. Zhang, W. Tang, and M. Shahidehpour, "Event-triggered updating method in centralized and distributed secondary controls for islanded microgrid restoration," *IEEE Trans. Smart Grid*, vol. 11, no. 2, pp. 1387–1395, Mar. 2020.
[19] F. Guo, Q. Xu, C. Wen, L. Wang, and P. Wang, "Distributed secondary control for power allocation and voltage restoration in islanded DC microgrids," *IEEE Trans. Sustain. Energy*, vol. 9, no. 4, pp. 1857–1869, Oct. 2018.
[20] J. Liu, J. Li, H. Song, A. Nawaz, and Y. Qu, "Nonlinear secondary voltage control of islanded microgrid via distributed consistency," *IEEE Trans. Energy Convers.*, vol. 35, no. 4, pp. 1964–1972, Dec. 2020.
[21] S. Liu, X. Wang, and P. X. Liu, "Impact of communication delays on secondary frequency control in an islanded microgrid," *IEEE Trans. Ind. Electron.*, vol. 62, no. 4, pp. 2021–2031, Apr. 2015.
[22] G. Lou, W. Gu, Y. Xu, W. Jin, and X. Du, "Stability robustness for secondary voltage control in autonomous microgrids with consideration of communication delays," *IEEE Trans. Power Syst.*, vol. 33, no. 4, pp. 4164–4178, Jul. 2018.
[23] Z. Zhang, C. Dou, D. Yue, and B. Zhang, "Predictive voltage hierarchical controller design for islanded microgrids under limited communication," *IEEE Trans. Circuits Syst. I, Reg. Papers*, vol. 69, no. 2, pp. 933–945, Feb. 2022.
[24] A. Lasheen, M. E. Ammar, H. H. Zeineldin, A. Al-Durra, M. F. Shaaban, and E. El-Saadany, "Assessing the impact of reactive power droop on inverter based microgrid stability," *IEEE Trans. Energy Convers.*, vol. 36, no. 3, pp. 2380–2392, Sep. 2021.
[25] F. Léonard, "Delay approximation comparison in a CACSD context," *IFAC Proc. Volumes*, vol. 31, no. 19, pp. 87–92, Jul. 1998.

**AHMED LASHEEN** was born in Giza, Egypt. He received the Graduate degree and the M.Sc. and Ph.D. degrees in electrical engineering from Cairo University, Giza, in 2010, 2013, and 2017, respectively. He is currently an Associate Professor with Cairo University. His current research interests include wind energy conversion systems, microgrids, model predictive control, fuzzy control, adaptive control, autonomous vehicles, and neural networks.

**HATEM F. SINDI** (Senior Member, IEEE) received the B.Sc. degree in electrical engineering from King Abdulaziz University, Jeddah, Saudi Arabia, in 2007, and the M.Sc. and Ph.D. degrees in electrical engineering from the University of Waterloo, Waterloo, ON, Canada, in 2013 and 2018, respectively. He is currently an Assistant Professor with the Department of Electrical and Computer Engineering, King Abdulaziz University. His research interests include smart grid, renewable DG, and distribution system planning.

**MAJID NOUR** received the bachelor's degree in electrical engineering (biomedical) from King Abdul Aziz University, in 2007, the master's degree in biomedical engineering from La Trobe University, Australia, in 2010, and the Ph.D. degree in electronics engineering (biomedical) from the Royal Melbourne Institute of Technology (RMIT), Australia, in 2014. He is currently an Associate Professor with KAU and an active researcher in the field of nanotechnology, biomedical engineering, and sensors with several highly cited publications. He is keen in innovation, technology transfer, hospital design, regulation, and standards. He is a medical equipment and hospital design consultant.

**MOSTAFA F. SHAABAN** (Senior Member, IEEE) received the B.Sc. and M.Sc. degrees in electrical engineering from Ain Shams University, Cairo, Egypt, in 2004 and 2008, respectively, and the Ph.D. degree in electrical engineering from the University of Waterloo, Waterloo, ON, Canada, in 2014. He is currently an Associate Professor with the Department of Electrical Engineering, American University of Sharjah, Sharjah, United Arab Emirates, and an Adjunct Professor with the University of Waterloo, Waterloo, ON, Canada. He has several publications in international journals and serves as an Associate Editor for *IET Smart Grid* and a reviewer for several refereed journals. His research interests include smart grid, renewable DG, distribution system planning, and electric vehicles.

**AHMED OSMAN** (Senior Member, IEEE) received the B.Sc. and M.Sc. degrees in electrical engineering from Helwan University, Cairo, Egypt, in 1991 and 1996, respectively, and the Ph.D. degree in electrical engineering from the University of Calgary, Calgary, AB, Canada, in 2003. From 2004 to 2008, he was an Assistant Professor with the Department of Electrical and Computer Engineering, University of Calgary. He is currently a Professor with the Department of Electrical Engineering, American University of Sharjah, Sharjah, United Arab Emirates. His research interests include power system analysis and power system protection.

**HATEM H. ZEINELDIN** (Senior Member, IEEE) received the B.Sc. and M.Sc. degrees in electrical engineering from Cairo University, Giza, Egypt, in 1999 and 2002, respectively, and the Ph.D. degree in electrical and computer engineering from the University of Waterloo, Waterloo, ON, Canada, in 2006. He was with Smith and Andersen Electrical Engineering Inc., North York, ON, USA, where he was involved in projects involving distribution system designs, protection, and distributed generation. He was a Visiting Professor with the Massachusetts Institute of Technology, Cambridge, MA, USA. He is currently with the Khalifa University of Science and Technology, Abu Dhabi, United Arab Emirates, and on leave from the Faculty of Engineering, Cairo University. His current research interests include distribution system protection, distributed generation, and micro grids. He is also an Editor for the IEEE TRANSACTIONS ON ENERGY CONVERSION.